HO_2NO_2 and HNO_3 in the coastal Antarctic winter night: A "lab-in-the-field" experiment

A.E. Jones, N. Brough, P.S. Anderson[*], E.W. Wolff[**]

British Antarctic Survey, Natural Environment Research Council, Cambridge, UK

[*] Now at Scottish Association of Marine Science, Scottish Marine Institute, Oban, UK

[**] Now at Dept of Earth Sciences, University of Cambridge, UK

Corresponding author:

Dr. A.E. Jones,

British Antarctic Survey,

High Cross,

Madingley Road,

Cambridge,

CB3 0ET, UK

e-mail: aejo@bas.ac.uk

Tel: +44 1223 221435

Fax: +44 1223 221279

Categories (for ACP Editorial Assignment):

Subject area: Gases

Research Activity: Field Measurements

Altitude Range: Troposphere

Science Focus: Chemistry

Abstract

Observations of peroxynitric acid (HO_2NO_2) and nitric acid (HNO_3) were made during a 4 month period of Antarctic winter darkness at the coastal Antarctic research station, Halley. Mixing ratios of HNO_3 ranged from instrumental detection limits to ~8 parts per trillion by volume (pptv), and of HO_2NO_2 from detection limits to ~5 pptv; the average ratio of HNO_3:HO_2NO_2 was 2.0(±0.6):1, with HNO_3 always present at greater mixing ratios than HO_2NO_2 during the winter darkness. An extremely strong association existed for the entire measurement period between mixing ratios of the respective trace gases and temperature: for HO_2NO_2, R^2 = 0.72, and for HNO_3, R^2 = 0.70. We focus on three cases with considerable variation in temperature, where wind speeds were low and constant, such that, with the lack of photochemistry, changes in mixing ratio were likely to be driven by physical mechanisms alone. We derived enthalpies of adsorption (ΔH_{ads}) for these three cases. The average ΔH_{ads} for HNO_3 was -42±2 kJ.mol^{-1} and for HO_2NO_2 was -56±1kJ.mol^{-1}; these values are extremely close to those derived in laboratory studies. This exercise demonstrates i) that adsorption to/desorption from the snow pack should be taken into account when addressing budgets of boundary layer HO_2NO_2 and HNO_3 at any snow-covered site, and ii) that Antarctic winter can be used as a natural "laboratory in the field" for testing data on physical exchange mechanisms.

1 Introduction

Peroxy nitric acid (HO_2NO_2, also written as HNO_4) and nitric acid (HNO_3) are acidic gases that are of increasing interest to polar tropospheric chemistry. Their primary relevance is that they act as reservoir species for HOx and NOx, which are now recognised to drive the surprisingly vigorous oxidation chemistry that has been observed during Antarctic summer (e.g. Davis et al., 2001; Chen et al., 2001). The spatial and temporal distribution of $HO_2NO_2$and HNO_3 across the polar regions thus becomes important for understanding the overall atmospheric chemical system, and models require details of their sources, and any physical exchange process by which they move from one environmental compartment to another. Currently, many of these details are unknown.

The gas-phase chemistry of HO_2NO_2 and HNO_3 is relatively straightforward. Peroxy nitric acid is a somewhat unstable molecule that forms and dissociates through its temperature-dependent equilibrium reaction:

$$HO_2 + NO_2 + M \leftrightarrow HO_2NO_2 + M \qquad \text{R1, -1}$$

which renders an increased stability for HO_2NO_2 at lower temperatures.

There are a number of photodissociation pathways which drive HO_2NO_2 and HNO_3 chemistry under sunlit conditions. The most important are thought to be:

$$HO_2NO_2 + h\nu \rightarrow HO_2 + NO_2 \qquad \text{R2a}$$

$$\rightarrow OH + NO_3 \qquad \text{R2b}$$

Peroxynitric acid can also be lost through reaction with OH:

$$HO_2NO_2 + OH \rightarrow H_2O + NO_2 + O_2 \qquad \text{R3}$$

Gas-phase production of nitric acid proceeds via:

$$OH + NO_2 + M \rightarrow HNO_3 + M \qquad \text{R4}$$

The major loss processes are reaction with OH and photolysis:

$$HNO_3 + OH \rightarrow H_2O + NO_3 \qquad \text{R5}$$

$$HNO_3 + h\nu \rightarrow OH + NO_2 \qquad \text{R6}$$

Both HO_2NO_2 (Ulrich et al., 2012) and HNO_3 (Bartels-Rausch et al., 2002; Hudson et al., 2002; Ullerstam et al., 2005) have been shown in laboratory experiments to adsorb to ice surfaces. This conclusion is supported by field observations which have confirmed uptake of both HNO_3 and HO_2NO_2 to snow surfaces (Huey et al., 2004; Slusher et al., 2002), and of HNO_3 to cirrus clouds (Weinheimer et al., 1998; Popp et al., 2004; Ziereis et al., 2004). In general, therefore, in snow covered areas, or indeed regions of the atmosphere with lofted snow/ice, such as cirrus clouds or blowing/precipitating snow, physical adsorption of HNO_3 and HO_2NO_2 from the air to the snow/ice is likely to occur. The details of this uptake will differ somewhat between the two molecules because

the partitioning coefficient of HNO_3 is greater than that for HO_2NO_2. HNO_3 is thus more sticky than HO_2NO_2, and a higher fraction of HNO_3 can be expected on the ice surface compared with HO_2NO_2.

High resolution observations of HNO_3 and HO_2NO_2 in the polar regions are scarce. Critically, both HO_2NO_2 and HNO_3 have been measured together during a number of Antarctic studies at high temporal resolution. These studies have included both ground-based experiments at South Pole (Slusher et al., 2002; Huey et al., 2004) and airborne measurements across the wider Antarctic Plateau (Slusher et al., 2010).

The ground-based studies have revealed considerable inter-annual variability in summertime HNO_3 and HO_2NO_2 mixing ratios, but always of the order 10s pptv at the South Pole. For example, the median observed HNO_3 between 16 and 31 December in 2000 was 18.2 pptv and for HO_2NO_2 was 23.5 pptv (Davis et al., 2004); over the equivalent time period in 2003, the median HNO_3 was 84 pptv, and for HO_2NO_2 was 39 pptv (Eisele et al., 2008). Considerably greater mixing ratios have also been observed; for example, the median mixing ratio of HNO_3 between 15 and 30th November 2003 was 194 pptv, and of HO_2NO_2 was 63 pptv (Eisele et al., 2008). While the specific mixing ratios will be strongly influenced by boundary layer height, overall, these high mixing ratios are fuelled by in situ production from elevated levels of NO_x and HO_x within the South Pole boundary layer, in turn driven by photochemical release of trace gases from the surrounding snowpack (Davis et al., 2001, 2008).

The airborne measurements assessed the three-dimensional distribution of HO_2NO_2 and HNO_3 across the Antarctic Plateau during the ANTCI 2005 campaign (Slusher et al., 2010). They revealed significant vertical gradients in both species, with higher concentrations at the ground, consistent with a source associated with emissions from the snowpack. The measurements also showed a widespread distribution of both HNO_3 and HO_2NO_2 across the Plateau region.

To date there have been no measurements of high temporal resolution HO_2NO_2 and HNO_3 in coastal Antarctica, and no measurements at all from Antarctica outside the summer season. We report here observations of HO_2NO_2 and HNO_3 made using a chemical ionisation mass spectrometer (CIMS) at Halley research station in coastal Antarctica (75^o 35' S, 26^o 39' W) from 24 May to 18 September 2007. The data allow us to assess whether HNO_3 and HO_2NO_2 are present in significant concentrations at other Antarctic locations and seasons than the Antarctic Plateau in summer. They also provide an opportunity to test laboratory-derived physical exchange parameters under semi-constrained, but genuine real-world conditions. At Halley, the sun remains below the horizon from April 30th to August 13th, such that this new data set includes many weeks of winter darkness. Under these conditions of 24 hour per day darkness, atmospheric photochemistry stalls, and trace gas concentrations are controlled entirely by either transport or physical air-snow exchange.

2 Experimental

2.1 CIMS instrumentation

The CIMS instrument used in this study has been described in detail elsewhere (Buys et al., 2013). It was installed in the Clean Air Sector Laboratory (CASLab), which is located roughly 1 km from the

main Halley station, and in a sector that rarely receives air from the base (Jones et al 2008). The CIMS inlet extended ~20 cm above the roof of CASLab, at a height roughly 5 m above the surrounding snowpack. The inlet system was designed to minimise residence time and surface losses (Neuman et al., 1999).

The instrument employed the SF_6^- method to detect both HNO_3 and HO_2NO_2, using the NO_4^-(HF) cluster at m/z 98 to detect HO_2NO_2, and NO_3^-(HF) at m/z 82 to detect HNO_3 (as per Slusher et al., 2001, 2002). Calibration was achieved using the SO_2 method as described by Slusher et al. (2001) and Kim et al. (2007). Background measurements, or zeros, were obtained every 10 minutes. These were achieved by passing sampled air for 3 minutes through a customized filter filled with activated coarse charcoal and nylon glass wool coated in $NaHCO_3$. This scrubbing method has previously been shown to be efficient at removing both HO_2NO_2 and HNO_3 from sampled air (Slusher et al., 2001). The instrument detection limit derived from background data averaged over 10-minutes was 0.7 pptv for HNO_3 and 0.4 pptv for HO_2NO_2. Total estimated uncertainty in the CIMS observations is ±40%.

While the SF_6^- method has been used successfully in previous field campaigns (e.g. Slusher et al., 2002; Slusher et al., 2010), it has been demonstrated in laboratory studies (Slusher et al., 2001) that SF_6^- reacts with H_2O in the sample air flow. This introduces an interferent into the technique, the non-linearity of which is evident in the unfiltered data (not shown). However, with their instrument reaction time of ~25 ms, Slusher et al. (2001) also concluded that this interferent was significant only at dewpoints greater than -25^{o}C, and that at lower dewpoints, the interferent was negligible. During the period of measurements at Halley, the CIMS instrument also operated with a reaction time of ~25 ms, such that the interferent would be equivalent to that of Slusher et al. (2001). At Halley, dewpoint temperatures varied from -12^{o}C to -52^{o}C (mean -31^{o}C), but were below -25^{o}C for 81% of the time. To remove the potential for H_2O interference in our data, all measurements made at dewpoints above -25^{o}C are filtered out from the dataset.

2.2 Boundary layer meteorology

Measurements of near-surface boundary layer meteorology were made on a 32-m profiling mast located ~25 m from the CASLab. Bulk sensors were located at 1, 2, 4, 8, 16, and 32 m above ground level, recording at 1Hz and averaged to 10 minute means; temperatures and humidity were measured with platinum resistance thermometers (0.1 K resolution) and solid state humidity probes (2% resolution), respectively, using an aspirated HMP35D from Vaisala Corp. 10 minute vector average wind speed and direction were measured with R.M. Young propeller vanes at 0.1 ms^{-1} and 2^o resolution .

Three 3-axis Metek USA-1 ultrasonic anemometer/thermometers were deployed at the 4, 16, and 32-m levels, sampling at 20 Hz. The data were tilt corrected and the relevant co-variances calculated over 1 minute means.

3 Results and discussion

145 **3.1 Overall data series**

146 The time series of filtered HO_2NO_2 and HNO_3 data, averaged to hourly means, is shown in Figure 1,
147 together with hourly means of ambient temperature, dew point temperature, and solar zenith
148 angle. The solar zenith angle shows that the sun was below the horizon for the majority of this time
149 period, and observations of NO and NO_2 (made using a Sonoma Tech. Dual channel
150 chemiluminescence analyser (Bauguitte et al., 2012; Cotter et al., 2003), with detection limits of 2
151 pptv for NO and 6 pptv for NO_2, not shown) were consistently below the instrumental detection
152 limits.

153 Regardless of this apparent lack of photochemical activity, there is considerable variability in the
154 HNO_3 and HO_2NO_2 observations. Mixing ratios of HNO_3 ranged from instrumental detection limits to
155 ~8 parts per trillion by volume (pptv) and of HO_2NO_2 varied from detection limits to ~5 pptv. These
156 values are considerably lower than those observed at South Pole in summer, where photochemical
157 production is fuelled by emissions of NOx from the snowpack, and where mixing ratios of HNO_3 and
158 HO_2NO_2 were generally in the 10s of pptv, and sometimes over 100 pptv, as discussed earlier.

159 It is also noticeable in the Halley data that the pattern of variability in both HO_2NO_2 and HNO_3 was
160 very similar, with each time series tracking the other closely. Indeed the correlation between the
161 two chemical species was high, as shown in Fig. 2, where the correlation coefficient, R^2, for the
162 hourly averages was 0.70. This finding is consistent with the data of Slusher et al., (2002), which
163 showed that, although the range of mixing ratios at South Pole in summer were considerably higher
164 than observed at Halley during the winter (<5 to 54 pptv for HO_2NO_2, and <5 pptv to 68 pptv for
165 HNO_3), the variability observed in both species during the measurement period was, again, highly
166 coupled.

167 The timeseries presented in Fig. 1 also clearly shows the very strong association between mixing
168 ratios of HNO_3 and HO_2NO_2 and ambient (and dewpoint) temperature. This association is further
169 demonstrated in Fig. 3, which shows both HNO_3 and HO_2NO_2 plotted against ambient temperature,
170 again for the entire period of measurements. Calculated correlation coefficients with temperature
171 are high, with R^2 = 0.70 and 0.72 for HNO_3 and HO_2NO_2 respectively.

172 Given that mixing ratios of HNO_3 and HO_2NO_2 are so strongly associated with ambient temperature,
173 Table 1 gives the mean and standard deviation of HNO_3 and HO_2NO_2 measured between 24 May and
174 18 September 2007, calculated within specific temperature ranges. The statistics are derived using
175 only the filtered data that were above 3-sigma detection limits. At South Pole during the summer,
176 ambient temperature ranged from -31.5^{o}C to -23.6^{o}C, with a mean of -27.7^{o}C; within this
177 temperature range, HNO_3 mixing ratios ranged from <5 to 54 pptv (mean 25 pptv) and HO_2NO_2
178 ranged from <5 to 68 pptv (mean 22pptv). For the equivalent temperature range at Halley (also with
179 a mean of -27.7^{o}C), mean and maximum mixing ratios for HNO_3 were 4.4 pptv and 9 pptv
180 respectively, and for HO_2NO_2 were 2.5 pptv and 5 pptv respectively, clearly significantly below those
181 observed at South Pole, for the reasons outlined above.

182 Differences between South Pole summer and Halley winter are also evident in the ratio of
183 HNO_3:HO_2NO_2, arising through differences in the species' lifetimes. Throughout the Halley
184 measurement period, the average ratio of HNO_3:HO_2NO_2 was 2.0(±0.6):1, with HNO_3 always (apart

from a few outliers) present at greater mixing ratios than HO_2NO_2 during the winter darkness (see Fig. 4). This finding is in contrast to observations from South Pole during sunlit summer time, when mixing ratios of HNO_3 and HO_2NO_2 were roughly equal for much of the measurement period (Slusher et al., 2002). Figure 1 of Slusher et al. (2002) shows that HO_2NO_2 was present at higher mixing ratios than HNO_3 for roughly 2 out of the 7 days of measurements; during the roughly 4 months of measurements at Halley, the only occasion when the mixing ratio of HO_2NO_2 exceeded that of HNO_3 was on the 6th and 7th September, a period when temperatures were particularly low but there was a limited amount of sunlight.

3.2 Short-term variability in HNO_3 and HO_2NO_2 and link to ambient temperature

The short-term variability in the HNO_3 and HO_2NO_2 is shown more clearly in Figure 5. The three examples show periods when ambient air temperatures varied rapidly and considerably, but where they remained below the -25°C dewpoint threshold such that no chemical data filtering was required. These 10-minute averages show that even very small-scale features of temperature change are reflected in the chemical measurements. For example, at midnight on 5th June, the short-lived peak in temperature is reflected also in HNO_3 and HO_2NO_2; the temperature peak around 11am on 21st June is apparent with similar, small, peaks in HNO_3 and HO_2NO_2; and the short-lived temperature peak around noon on 15th July is also evident in short-lived increases in HNO_3 and HO_2NO_2 mixing ratios. While large-scale variability in HNO_3 and HO_2NO_2 could be linked to air mass origin, such fine-scale variability can only be explained by a local, fast-acting, source/sink mechanism. The association between variability in HNO_3 and HO_2NO_2 and changes in ambient temperature strongly suggest a temperature-dependent mechanism. Given our understanding of the interaction between acidic gases and ice gained through laboratory studies (e.g. Huthwelker et al., 2006), one possible mechanism is temperature-dependent adsorption/desorption at the snow surface.

3.3 Evidence for HO_2NO_2 and HNO_3 air/snow exchange

To probe in more detail the response of HNO_3 and HO_2NO_2 to changes in temperature, we examined periods in the data where ambient temperatures changed, but where wind speeds were relatively low and invariable. By adopting this approach, we minimise any influence that air flow through the snow (e.g. via ventilation/wind pumping) may have on air/snow exchange processes. We derive a mixing diffusivity to determine the timescale for vertical mixing (via turbulent diffusion) between the snow surface and the CIMS inlet height, in order to confirm that the CIMS HNO_3 and HO_2NO_2 observations can be used to analyse processes occurring at the ground-level air/snow interface. The mixing diffusivity is roughly equal to $k.z.u_*$, where k = von Karman's constant (=0.4), z = CIMS inlet height (=5 m) and u_*, the friction velocity, is derived from the sonic anemometer data (Stull 1988). The e-folding time scale, t_{sc}, is given by z^2/diffusivity, that is $t_{sc} = z/(k.u_*)$. t_{sc} will vary during each case study, but cannot be negative: this range is presented below derived from log means and standard deviations. Figure 6a shows observations made on 30th May 2007, with a clear gradual increase in both HNO_3 and HO_2NO_2 as ambient temperatures rose from ~-44°C to ~-30°C. On this day, data from

the boundary layer mast (not shown) show that between the surface and 8 m height, there was little or no temperature gradient; to first order, therefore, 8 m temperatures can be used as a surrogate for those at the ground. Wind speeds were between 0 and 2 ms^{-1} from the surface to 4 m, and remained at around 2 $m.s^{-1}$ at 8 m height. For 95% of the time, t_{sc} was between 100 s and 300 s.

Figure 6b) shows data for the period from 9am to midnight on 21st June, discussed briefly in section 3.2 above. Again, a gradual increase in mixing ratios of HNO_3 and HO_2NO_2 is evident (upper panel), as ambient temperatures rose gradually from ~-38°C to ~-26°C. Data from the boundary layer met mast show that, during this period, there was no vertical gradient in temperature between the surface and 8 m height; wind speeds from the surface to 8 m were below 2 ms^{-1}. Data from the sonic anemometers show that vertical mixing was again very weak, with mixing time scales between 90 s and 600 s.

Figure 6c) shows observations from midnight to 9am on 18th July, another quiescent period, with wind speeds in the lowest 8 m below 1 ms^{-1}, and with no temperature gradient below 32 m. Gradual increases in both HNO_3 and HO_2NO_2 proceed as ambient temperatures rise from -38°C to -30°C. t_{sc} varied between 30 s and 100 s during the event.

Correlation coefficients between mixing ratios of HNO_3 (and HO_2NO_2) and temperature, are extremely high for the time periods presented in Figure 6: R^2 for the correlation between HNO_3 and temperature is 0.72 (30th May), 0.90 (21st June) and 0.72 (18th July); for the correlation between HO_2NO_2 and temperature, R^2 was 0.88 (30th May), 0.94 (21st June), and 0.92 (18th July). The values of R^2 show that between 72% and 90% of the variability in HNO_3 can be explained by variability in temperature; and between 88% and 94% of the variability in HO_2NO_2 can be explained by the variability in temperature.

3.4 Deriving enthalpy of adsorption from the Halley field data

The enthalpies of adsorption between HNO_3/ice and HO_2NO_2/ice have been derived in laboratory experiments carried out under environmentally-relevant conditions. Ulrich et al. (2012) studied uptake of HO_2NO_2 at low concentrations and temperatures between 230 K and 253 K while Bartels-Rausch et al. (2002) and Ullerstam et al. (2005) studied the adsorption enthalpy of HNO_3. Field studies carried out during the 24-hour per day darkness of Antarctic winter provide optimum conditions for validating such laboratory-derived physical air/snow exchange parameters under "real-world" conditions.

At equilibrium, the partitioning of HO_2NO_2 or HNO_3 molecules between the gas phase (C_g) and the snow/ice surface (C_s) can be expressed as:

$$K_{part} = \frac{C_s}{C_g}$$

As the partition constant will obey the van't Hoff equation, a new equation can be written:

$$\frac{dlnK_{part}}{d\frac{1}{T}} = -\frac{\Delta H_{ads}}{R}$$

where T is the temperature (K), Δ*H* is the enthalpy of adsorption (J/mol), R is the gas constant (8.314 $J.K^{-1}.mol^{-1}$)

Given our definition of K_{part} above, the equation can then be re-formulated as:

$$\frac{dln\frac{C_s}{C_g}}{d\frac{1}{T}} = -\frac{\Delta H_{ads}}{R}$$

At 240 K, roughly the temperatures of our observations, Ulrich et al. (2012), in their Figure 4, show $C_s/C_g \approx 20$ cm for HO_2NO_2 and 8000 cm for HNO_3. In the firn, the ratio of the surface area of snow to the volume of air is approximately 0.5 to 5 cm^{-1} (based on a density of snow of 0.3 g cm^{-3} and a specific surface area of 100 to 1,000 cm^2g^{-1} (Domine et al., 2008)). We can therefore calculate that the ratio of the number of molecules of HNO_3 adsorbed to the snow surface to that in the gas phase, is approximately 4 x 10^5 to 4 x 10^6; for HO_2NO_2, this ratio is 1000 to 10,000. As a result, for both HNO_3 and HO_2NO_2, exchange between the air and snow will thus have little effect on C_s, which can therefore be considered as a constant relative to C_g.

If we also assume that, over several hours, and under low and constant wind conditions, the concentration at our inlet tracks the concentration in the firn, then:

$$\frac{dlnC_g}{d\frac{1}{T}} = \frac{\Delta H_{ads}}{R}$$

It is then possible to derive ΔH_{ads} from the slope of lnC_g vs 1/T multiplied by R.

For the Halley data, Figure 7 shows plots of both $ln(HNO_3)$ vs 1/T and $ln(HO_2NO_2)$ vs 1/T for the time periods discussed in section 3.3 above. As a reminder, these periods are characterised by 24-hour per day darkness, low wind speeds, and limited vertical mixing from turbulent diffusion, so are as close to laboratory conditions as could be found in our dataset. They were also chosen as they spanned a reasonably large temperature range, which would improve the constraint on the linear fit.

The values of ΔH_{ads} derived from these fits are given in Table 2. The average ΔH_{ads} for HNO_3 is -42±2 $kJ.mol^{-1}$ which can be compared with laboratory-derived values of Bartels-Rausch et al. (2002) and Ullerstam et al. (2005). Bartels-Rausch et al. (2002) derived ΔH_{ads} of -44 $kJ.mol^{-1}$ (with random error 2.3 $kJ.mol^{-1}$, systematic error 13 $kJ.mol^{-1}$); Ullerstam et al. (2005), working at lower concentrations of HNO_3, relevant to the natural atmosphere, derived ΔH_{ads} of -30.6 ± 6.0 $kJ.mol^{-1}$. For HO_2NO_2, the average ΔH_{ads} derived from our field data is -56±1 $kJ.mol^{-1}$ which can be compared with the laboratory-derived value (Ulrich et al., 2012) of -59 $kJ.mol^{-1}$. For both HO_2NO_2 and HNO_3, the agreement between laboratory and field-derived enthalpies of adsorption is remarkably good.

4. Summary and conclusions

We present the first high time resolution observations of HNO_3 and HO_2NO_2 in coastal Antarctica, and the first from Antarctica during the dark winter period. Mixing ratios of HNO_3 ranged from instrumental detection limits to ~8 parts per trillion by volume (pptv) and of HO_2NO_2 varied from detection limits to ~5 pptv. These values are on average lower than those observed at South Pole in summer, where mixing ratios of HNO_3 and HO_2NO_2 were generally in the 10s of pptv, and sometimes over 100 pptv.

The Antarctic, during winter, is an ideal natural laboratory for studying physical air/snow exchange processes. The environmental system is considerably simplified compared with other times of the year because of the lack of photochemical activity which must otherwise be taken into account when interpreting data.

In our study, we considered whether adsorption/desorption of HNO_3 and HO_2NO_2 to snow/ice surfaces could be invoked to explain our observations; we did not consider formation of solid solutions from solid ice, or take-up to liquid NaCl aerosols. In a follow-up study that further analysed our field data, Bartels-Rausch (2014) considered both the case of Langmuir adsorption to the ice surface, and solubility in ice forming a solid solution. He found that equilibrium air/snow partitioning was able to describe our field data well, both in terms of absolute mixing ratios and trend with temperature. He also found that the reservoir of adsorbed HNO_3 and HO_2NO_2 in the upper snow pack was sufficient to fuel the observed emissions. In contrast, while calculations based on reversible solid-solution/air partitioning were able to describe mixing ratios of HNO_3, they were not able to reproduce the observed trend with temperature. Further, the reservoir of HNO_3 in the outer part of the snow crystals was too small to explain observed increases in mixing ratio.

The measurements of HNO_3 and HO_2NO_2 from Halley are consistent with laboratory experiments showing a temperature-dependence in the partitioning of both HNO_3 and HO_2NO_2 to ice. They further support the conclusion that HO_2NO_2/ice interactions are stronger than those between HNO_3 and ice, as shown by the higher enthalpy of adsorption of HO_2NO_2 compared with HNO_3 (Ulrich et al., 2012). On short-timescales, therefore, HNO_3 and HO_2NO_2 that is adsorbed to snow/ice can be re-released as temperatures rise. The snowpack can thus act as a source of HNO_3 and HO_2NO_2 to the overlying atmosphere at all times of the year given sufficient reservoir in the snowpack and changing temperatures. Similarly, HNO_3 and HO_2NO_2 adsorbed to cirrus clouds would be desorbed should temperatures rise. Such a reversible, temperature-dependent partitioning also provides a mechanism for re-distributing HNO_3 and HO_2NO_2 on a local or regional scale across Antarctica. Snow can be transported considerable distances by storm systems, and adsorbed HO_2NO_2 and HNO_3 can be desorbed as a function of changing temperature experienced along the transport pathway. Indeed, transport of snow from inland Antarctica is likely to contribute to the HO_2NO_2 and HNO_3 reservoir in the coastal snowpack. The other likely source for HO_2NO_2 to the winter snowpack is the general shift in equilibria, as temperatures fall from summer to winter, from gas-phase HO_2 and NO_2 towards gaseous HO_2NO_2, and then, by temperature-dependent partitioning, towards snowpack-adsorbed HO_2NO_2.

While clearly a controlling mechanism during polar night, the importance of air/snow partitioning relative to photochemistry will vary according to time of year and location. However, adsorption to/desorption from the snow pack should be taken into account when addressing budgets of

boundary layer HO_2NO_2 and HNO_3 at any snow-covered site, as all are likely to experience varying ambient temperature which would drive such air/snow exchange.

Acknowledgements:

The authors thank Greg Huey and Dave Tanner for providing the CIMS instrument used in this work, and for their help in setting it up at Halley. AEJ thanks Robert Mulvaney for useful discussions around this work. The authors are also grateful for Thorsten Bartels-Rausch for discussions and his subsequent modelling calculations. This study is part of the British Antarctic Survey Polar Science for Planet Earth Programme. It was funded by The Natural Environment Research Council (NERC).

References

Bartels-Rausch, T., Eichler, B., Zimmermann, P., Gäggeler, H.W., and Ammann, M.: The adsorption of nitrogen oxides on crystalline ice, Atmos. Chem. Phys., 2, 235–247, doi:10.5194/acp-2-235-2002, 2002.

Bartels-Rausch, T.: Ice-air partitioning of HNO_3 and HNO_4 drives winter mixing ratio, Atmos. Chem. Phys. Discuss., 14, C4673–C4694, www.atmos-chem-phys-discuss.net/14/C4673/2014/ , 2014.

Bauguitte, S. J.-B., Bloss, W.J., Evans, M.J., Salmon, R.A., Anderson, P. S., Jones, A. E., Lee, J. D., Saiz-Lopez, A. , Roscoe, H. K., Wolff, E.W., and Plane, J. M. C., Summertime NOx measurements during the CHABLIS campaign: can source and sink estimates unravel observed diurnal cycles?, Atmos. Chem. Phys., 12, 989–1002, doi:10.5194/acp-12-989-2012, 2012.

Buys, Z., Brough, N., Huey, G., Tanner, D., von Glasow, R., and Jones, A. E.: High temporal resolution Br_2, BrCl and BrO observations in coastal Antarctica, Atmos. Chem. Phys., 13, 1329-1343, doi:10.5194/acp-13-1329-2013, 2013.

Chen, G., Davis, D., Crawford, J., Nowak, J.B., Eisele, F., Mauldin, R.L.., Tanner, D., Buhr, M., Shetter, R., Lefer, B., Arimoto, R., Hogan, A., and Blake, D.: An investigation of South Pole HOx chemistry: Comparison of model results with ISCAT observations, Geophys. Res. Lett., 28, 3633–3636, 2001.

Cotter, E.S.N., Jones, A.E., Wolff, E.W., Bauguitte, S.J.-B., What controls photochemical NO and NO_2 production from Antarctic snow? Laboratory investigation assessing the wavelength and temperature dependence, J. Geophys. Res., 108 (D4), 4147, doi:10.1029/2002JD002602, 2003.

Davis, D., Nowak, J.B., Chen, G., Buhr, M., Arimoto, R., Hogan, A., Eisele, F., Mauldin, L., Tanner, D., Shetter, R., Lefer, B., and McMurry, P.: Unexpected high levels of NO observed at South Pole, Geophys. Res Lett., 28(19), 3625–3628, 2001.

Davis, D., Chen, G., Buhr, M., Crawford, J., Lenschow, D., Lefer, B., Shetter, R., Eisele, F., Mauldin, L., and Hogan, A.: South Pole NOx chemistry: an assessment of factors controlling variability and absolute levels, Atmos. Environ., 38, 5375–5388, 2004.

Davis, D. D., Seelig, J., Huey, G., Crawford, J., Chen, G., Wang, Y., Buhr, M., Helmig, D., Neff, W., Blake, D., Arimoto, R., and Eisele, F.: A reassessment of Antarctic plateau reactive nitrogen based on ANTCI 2003 airborne and ground based measurements, Atmos. Environ., 42, 2831–2848, doi:10.1016/j.atmosenv.2007.07.039, 2008.

Domine, F., Albert, M., Huthwelker, T., Jacobi, H.-W., Kokhanovsky, A. A., Lehning, M., Picard, G., and Simpson, W.R.: Snow physics as relevant to snow photochemistry, Atmos. Chem. Phys., 8, 171–208, 2008.

Eisele, F., et al., Antarctic tropospheric chemistry investigation (ANTCI) 2003 overview, Atmos. Environ., 42(12), 2749‑2761, doi:10.1016/j.atmosenv.2007.04.013, 2008.

Hudson, P. K., Shilling, J. E., Tolbert, M. A., and Toon, O. B.: Uptake of nitric acid on ice at tropospheric temperatures: Implications for cirrus clouds, J. Phys. Chem. A, 106(42), 9874–9882, 2002.

Huey, L. G., Tanner, D. J., Slusher, D. L., Dibb, J. E., Arimoto, R., Chen, G., Davis, D., Buhr, M.P., Nowak, J. B., Mauldin, R. L., Eisele, F. L., and Kosciuch, E.: CIMS measurements of HNO_3 and SO_2 at the South Pole during ISCAT 2000, Atmos. Environ., 38, 5411–5421, 2004.

Huthwelker, T., Ammann, M., and Peter, T.: The uptake of acidic gases on ice, Chem. Rev., 106, 1375–1444, 2006.

Jones, A. E., Wolff, E. W., Salmon, R. A., Bauguitte, S. J.-B., Roscoe, H. K., Anderson, P. S., Ames, D., Clemitshaw, K. C., Fleming, Z. L., Bloss, W. J., Heard, D. E., Lee, J. D., Read, K. A., Hamer, P., Shallcross, D. E., Jackson, A. V., Walker, S. L., Lewis, A. C., Mills, G. P., Plane, J. M. C., Saiz-Lopez, A., Sturges, W. T., and Worton, D. R.: Chemistry of the Antarctic Boundary Layer and the Interface with Snow: an overview of the CHABLIS campaign, Atmos. Chem. Phys., 8, 3789–3803, doi:10.5194/acp-8-3789-2008, 2008.

Kim, S., Huey, L. G., Stickel, R. E., Tanner, D. J., Crawford, J. H., Olson, J. R., Chen, G., Brune, W. H., Ren, X., Lesher, R., Wooldridge, P. J., Bertram, T. H., Perring, A., Cohen, R. C., Lefer, B. L., Shetter, R. E., Avery, M., Diskin, G., and Sokolik, I.: Measurement of HO_2NO_2 in the free troposphere during the intercontinental chemical transport experiment – North America 2004, J. Geophys. Res.-Atmos., 112, D12S01, doi:10.1029/2006JD007676, 2007.

Neuman, J. A., Huey, L. G., Ryerson, T. B., and Fahey, D. W.: Study of inlet materials for sampling atmospheric nitric acid, Environ. Sci. Technol., 33, 1133– 1136, doi:10.1021/es980767f, 1999.

Popp, P. J., Gao, R. S., Marcy, T. P., Fahey, D. W., Hudson, P. K., Thompson, T. L., Karcher, B., Ridley, B. A., Weinheimer, A. J., Knapp, D. J., Montzka, D. D., Baumgardner, D., Garrett, T. J., Weinstock, E. M., Smith, J. B., Sayres, D. S., Pittman, J. V., Dhaniyala, S.., Bui, T. P., and Mahoney, M. J.: Nitric acid uptake on subtropical cirrus cloud particles, J. Geophys. Res., 109, D06302, doi:10.1029/2003JD004255, 2004.

Slusher, D. L., Pitteri, S. J., Haman, B. J., Tanner, D. J., and Huey, L. G.: A chemical ionization technique for measurement of pernitric acid in the upper troposphere and the polar boundary layer, Geophys. Res. Lett., 28, 3875–3878, doi:10.1029/2001GL013443, 2001.

Slusher, D. L., Huey, L. G., Tanner, D. J., Chen, G., Davis, D. D., Buhr, M., Nowak, J. B., Eisele, F. L., Kosciuch, E., Mauldin, R.L., Lefer, B. L., Shetter, R. E., and Dibb, J. E.: Measurements of pernitric acid at the South Pole during ISCAT 2000, Geophys. Res. Lett., 29, 2011, doi:10.1029/2002GL015703, 2002.

Slusher, D. L., Neff, W. D., Kim, S., Huey, L. G., Wang, Y., Zeng, T., Tanner, D. J., Blake, D. R., Beyersdorf, A., Lefer, B. L., Crawford, J. H., Eisele, F. L., Mauldin, R. L., Kosciuch, E., Buhr, M. P., Wallace, H. W., and Davis, D. D.: Atmospheric chemistry results from the ANTCI 2005 Antarctic plateau airborne study, J. Geophys. Res.-Atmos., 115, D07304, doi:10.1029/2009JD012605, 2010.

Stull, R.B., An Introduction to Boundary Layer Meteorology, Kluwer, Dordrecht, 1988.

Ullerstam, M., Thornberry, T., and Jonathan P. D. Abbatt, J.P.D.: Uptake of gas-phase nitric acid to ice at low partial pressures: evidence for unsaturated surface coverage, Faraday Discuss.**,** 130, 211-226, doi**:** 10.1039/B417418F, 2005.

418 Ulrich, T., Ammann, M., Leutwyler, S., and Bartels-Rausch, T.: The adsorption of peroxynitric acid on
419 ice between 230K and 253K, Atmos. Chem. Phys., 12, 1833–1845, doi:10.5194/acp-12-1833-2012,
420 2012.

421 Weinheimer, A. J., Campos, T. L., Walega, J. G., Grahek, F. E., Ridley, B. A., Baumgardner, D., Twohy,
422 C., and Gandrud, B.: Uptake of NOy on wave-cloud ice particles, Geophys. Res. Lett., 25(10), 1725–
423 1728, 1998.

424 Ziereis, H., Minikin, A., Schlager, H., Gayet, J. F., Auriol, F., Stock, P., Baehr, J., Petzold, A., Schumann,
425 U., Weinheimer, A., Ridley, B., and Strom, J.: Uptake of reactive nitrogen on cirrus cloud particles
426 during INCA, Geophys. Res. Lett., 31, L05115, doi:10.1029/2003GL018794, 2004.

Table 1. Mean and standard deviation of nitric acid and peroxy nitric acid according to ambient air temperature range. The statistics were derived using only data above the 3-sigma detection limit.

Table 2. The enthalpies of adsorption to ice for HO_2NO_2 and HNO_3 as derived from three periods of the Halley measurements. The number of observations used for each derivation is also given.

Fig. 1. Time series of HNO_3, HO_2NO_2, ambient temperature, dewpoint, and solar zenith angle (SZA) (hourly averages) for the entire measurement period discussed in this paper, 24 May 2007 to 18 September 2007.

Fig. 2. Nitric acid vs peroxy nitric acid; 1-houly averages of measurements made from 24 May 2007 to 18 September 2007.

Fig. 3. Nitric acid and peroxy nitric acid vs ambient temperature; 10-minute averages of measurements made from 24 May 2007 to 18 September 2007.

Fig. 4. Ratio of HNO_3 : HO_2NO_2 (hourly average data) for the May to September measurement period. Also shown, for reference, are ambient temperature and solar zenith angle.

Fig. 5. Three examples of short-term variability in HNO_3, HO_2NO_2 and ambient air temperature (10-minute data), from a) early June; b) mid June; c) mid July. All three periods are during the winter 24-hour per day darkness.

Fig. 6. Detail of changes in HNO_3, HO_2NO_2 and temperature on a) 30th May, b) 21st June, and c) 18th July. These three periods in the measurement series were characterised by low and invariant wind speeds and 24-hours per day darkness.

Fig. 7. Plots of ln(HNO_3) and ln(HO_2NO_2) vs 1/T for the time periods shown in Fig. 6, i.e. a) 30th May, b) 21st June, and c) 18th July.

Ambient air temperature (°C)	Nitric acid			Peroxy nitric acid		
	no. points	mean (pptv)	std. deviation	no. points	mean (pptv)	std. deviation
-45 to -47.4	24	0.96	0.12	0		
-40 to -45.9	579	1.36	0.42	472	0.58	0.14
-35 to -39.9	1575	2.13	0.74	1615	0.99	0.38
-30 to -34.9	3638	3.09	0.92	3732	1.6	0.44
-25 to -29.9	4821	4.32	1.18	4942	2.29	0.62
-21.2 to -24.9	1954	5.67	1.19	2013	3.23	0.62

448

449 Table 1. Mean and standard deviation of nitric acid and peroxy nitric acid according to ambient air
450 temperature range. The statistics were derived using only data above the 3-sigma detection limit.

451

	HO_2NO_2		HNO_3	
	ΔH_{ads}	no. observations	ΔH_{ads}	no. observations
30th May	-58 ± 2 kJ.mol^{-1}	144	-36 ± 2 kJ.mol^{-1}	144
21st June	-52 ± 2 kJ.mol^{-1}	90	-50 ± 2 kJ.mol^{-1}	82
18th July	-58 ± 2 kJ.mol^{-1}	55	-41 ± 4 kJ.mol^{-1}	55

452

453 Table 2. The enthalpies of adsorption to ice for HO_2NO_2 and HNO_3 as derived from three periods of
454 the Halley measurements. The number of observations used for each derivation is also given.

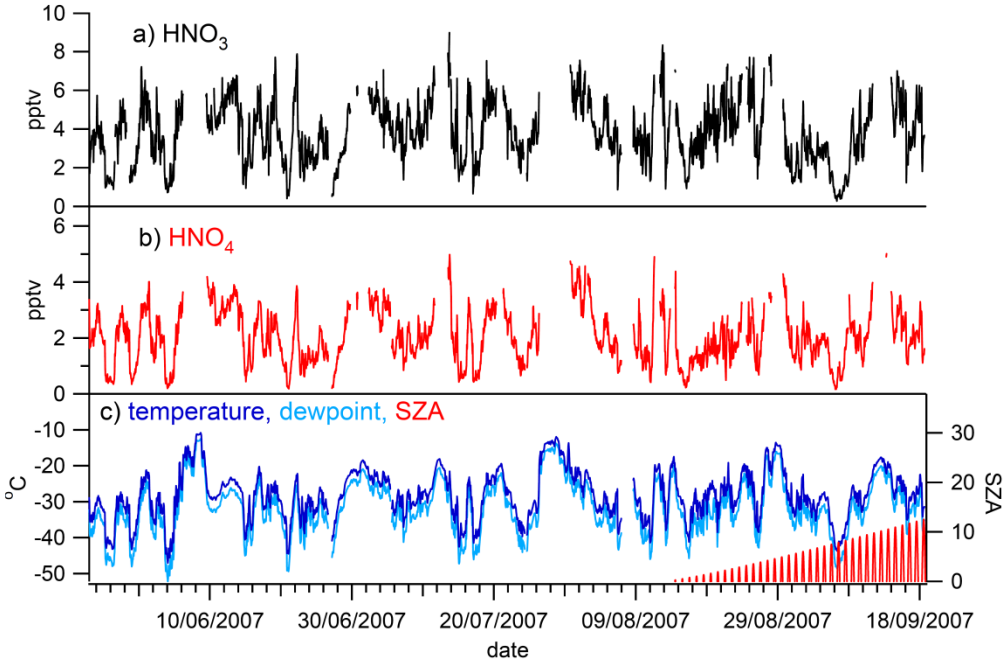

Fig. 1. Time series of HNO_3, HO_2NO_2, ambient temperature, dewpoint, and solar zenith angle (SZA) (hourly averages) for the entire measurement period discussed in this paper, 24 May 2007 to 18 September 2007.

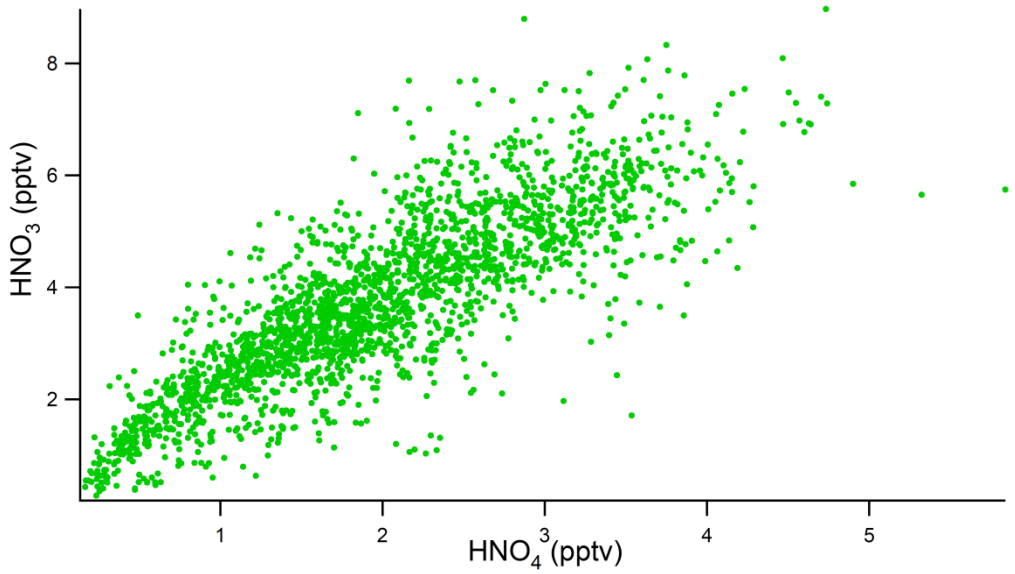

Fig. 2. Nitric acid vs peroxy nitric acid; 1-houly averages of measurements made from 24 May 2007 to 18 September 2007.

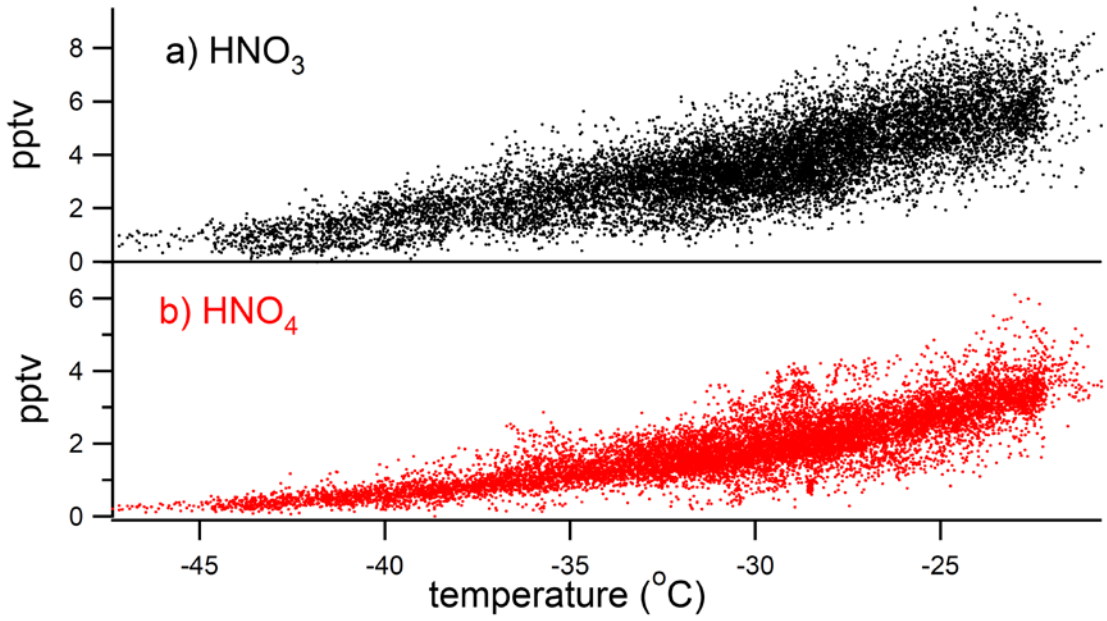

Fig. 3. Nitric acid and peroxy nitric acid vs ambient temperature; 10-minute averages of measurements made from 24 May 2007 to 18 September 2007.

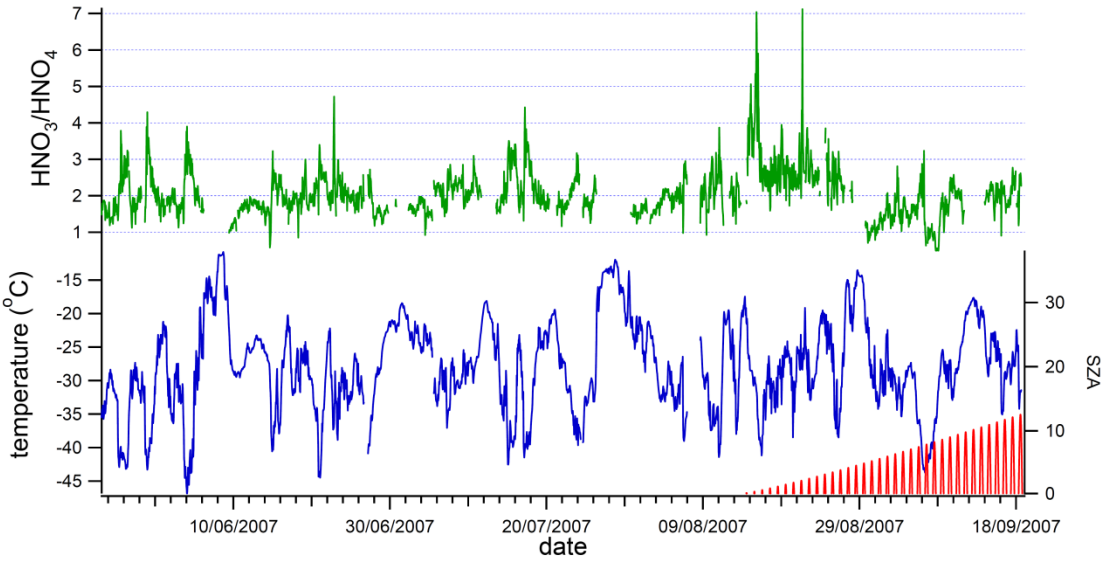

478

479 **Fig. 4.** Ratio of HNO_3 : HO_2NO_2 (hourly average data) for the May to September measurement
480 period. Also shown, for reference, are ambient temperature and solar zenith angle.

481

482

483

484

485

486

487

488

489

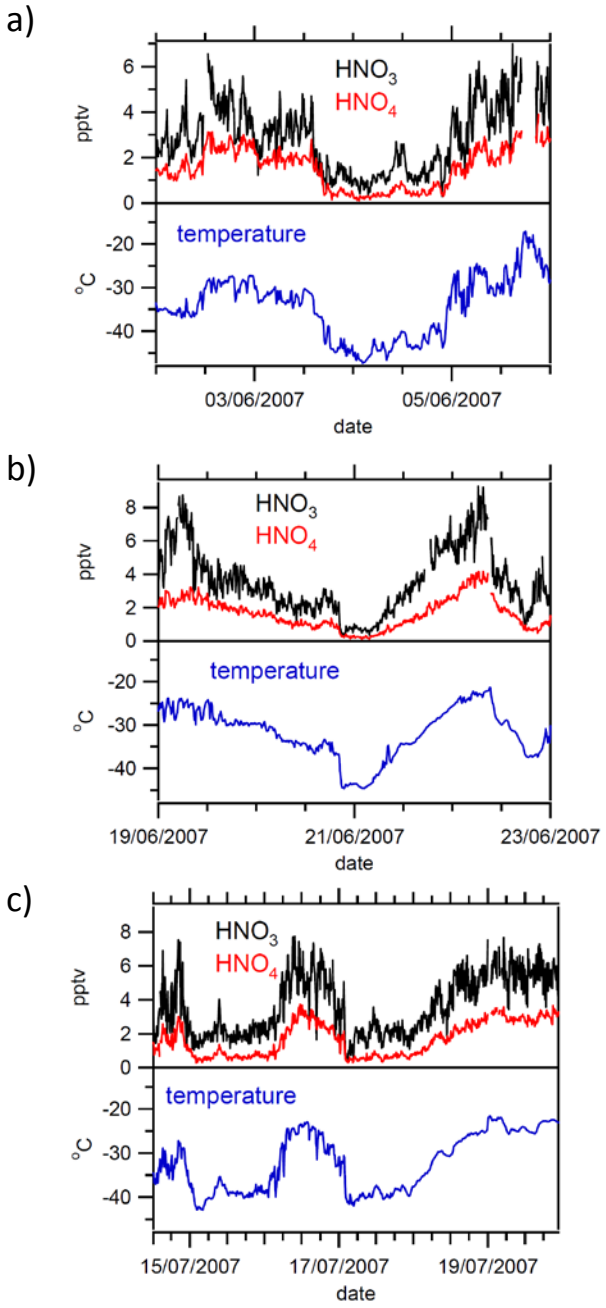

490

491 **Fig. 5.** Three examples of short-term variability in HNO_3, HO_2NO_2 and ambient air temperature (10-
492 minute data), from a) early June; b) mid June; c) mid July. All three periods are during the winter 24-
493 hour per day darkness.

494

495

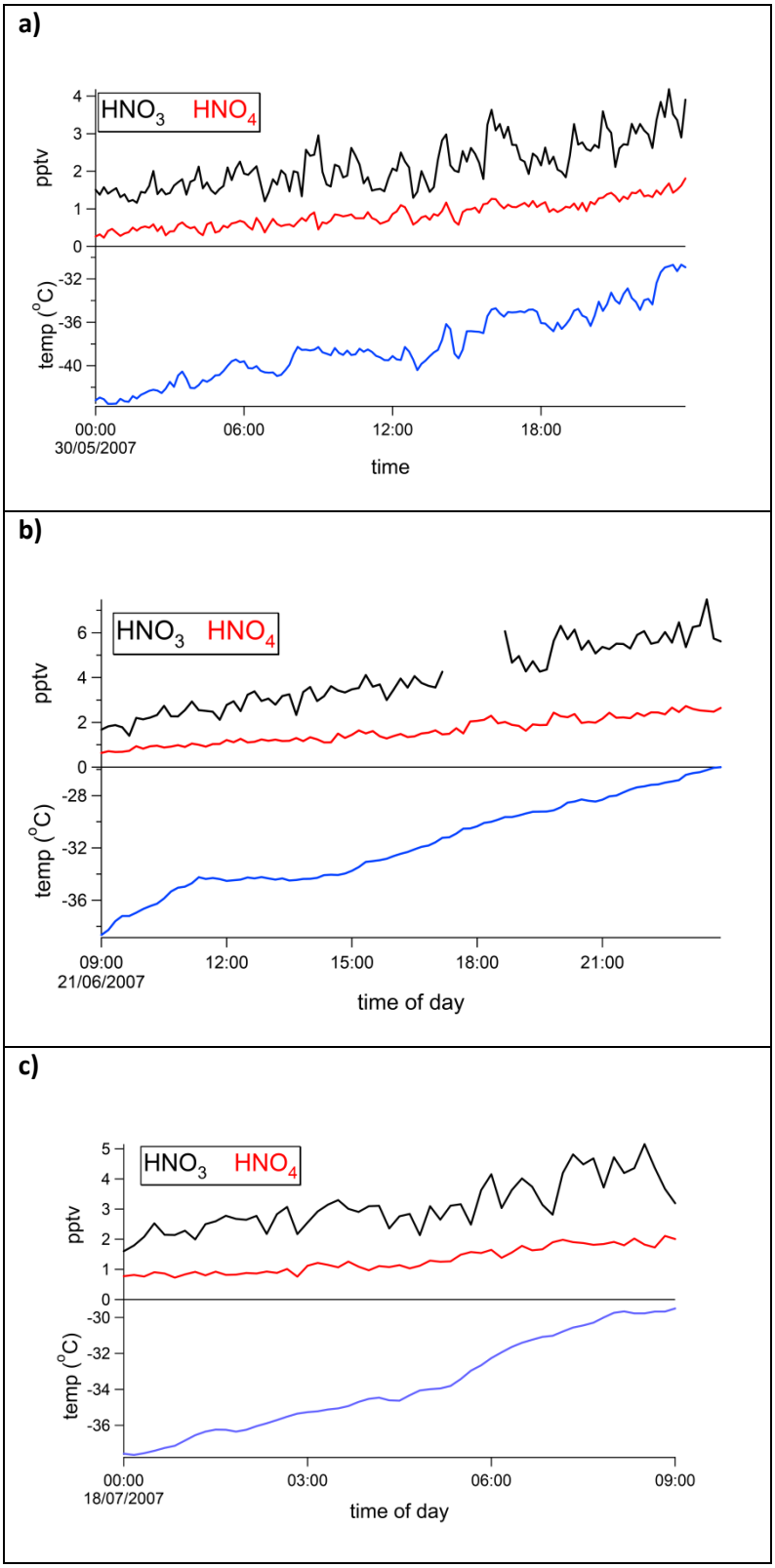

496

497 **Fig. 6.** Detail of changes in HNO_3, HO_2NO_2 and temperature on a) 30th May, b) 21st June, and c) 18th
498 July. These three periods in the measurement series were characterised by low and invariant wind
499 speeds and 24-hours per day darkness.

a)

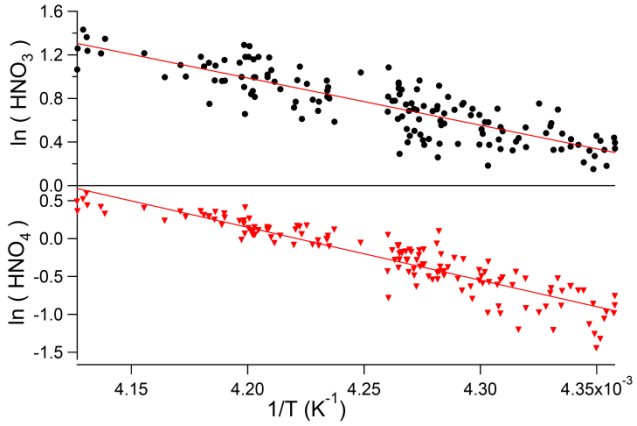

b)

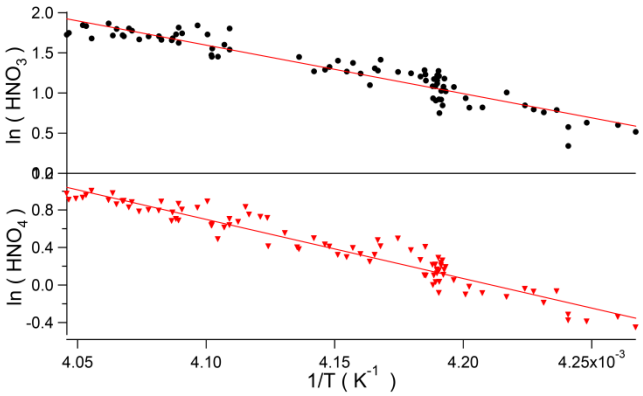

c)

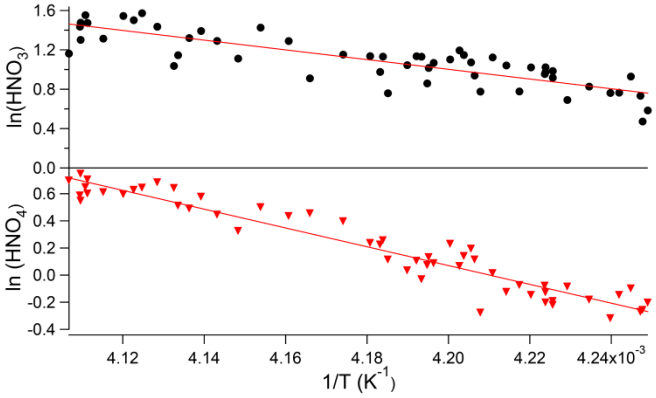

500

501 **Fig. 7.** Plots of ln(HNO_3) and ln(HO_2NO_2) vs 1/T for the time periods shown in Fig. 6, i.e. a) 30th May,
502 b) 21st June, and c) 18th July.

503